ELSEVIER

Chemical Engineering Science 60 (2005) 6430–6437

Chemical Engineering Science

www.elsevier.com/locate/ces

Mass transfer from Taylor bubbles rising in single capillaries

C.O. Vandu, H. Liu[1], R. Krishna*

Van 't Hoff Institute for Molecular Sciences, University of Amsterdam, Nieuwe Achtergracht 166, 1018 WV Amsterdam, The Netherlands

Received 23 October 2004; received in revised form 18 December 2004; accepted 21 January 2005
Available online 19 March 2005

Abstract

Gas–liquid mass transfer from Taylor bubbles rising in 1, 2 and 3 mm diameter capillaries of circular and square cross-sections was investigated for air–water system. The liquid-phase volumetric mass transfer coefficient k_La was obtained from experimental oxygen absorption dynamics. The experimental k_La values are in good agreement with the model developed by van Baten and Krishna (2004. Chemical Engineering Science 59, 2535–2545), with the additional assumption that the dominant mass transfer contribution is to the film surrounding the bubble.

Keywords: Mass transfer; Taylor bubbles; Vertical capillary; Penetration model; Monolith reactors

1. Introduction

The use of monolith reactors is becoming increasingly significant in view of several advantages such as low pressure drop, high mass transfer rates and ease of scaleup (Kreutzer, 2003; Stankiewicz, 2001). A monolith block is composed of an array of uniformly structured parallel channels often of circular or square geometry with dimensions typically in the range of 1–3 mm. Provided that a uniform distribution of the gas and liquid-phases occurs in the various channels of the monolith block, hydrodynamic and mass transfer data obtained from studies on a single channel can be employed in scaling up a monolith reactor. Of particular interest to the operation of monolith reactors is the Taylor flow regime, also known as the slug flow or bubble train flow regime. It is characterized by the presence of elongated gas bubbles with lengths greater than the channel diameter, which rise along the channel separated from each other by liquid slugs. For fast reactions, mass transfer from the Taylor bubbles to the surrounding liquid phase could become a limiting factor, requiring that the gas–liquid volumetric mass transfer coefficient k_La be reliably estimated (Kreutzer, 2003).

Bercic and Pintar (1997) put forward the following empirical correlation for the estimation of k_La in single channels based on experimental studies on the absorption of methane in water using circular capillaries of 1.5, 2.5 and 3.1 mm diameters.

$$k_La = 0.111\,\frac{(U_G + U_L)^{1.19}}{((1-\varepsilon_G)L_{UC})^{0.57}} \tag{1}$$

where U_G and U_L are the superficial velocities of the gas and liquid phases, ε_G is the gas hold-up, and L_{UC} is the unit cell length. It is remarkable to note that the Bercic–Pintar correlation for k_La shows no dependence on the channel diameter d_c. The liquid phase diffusivity Đ was not varied in their experiments and, consequently, does not appear in Eq. (1).

Irandoust and Andersson (1988), Irandoust et al. (1992), Kreutzer (2003) and van Baten and Krishna (2004) have adopted a more fundamental approach to the estimation of k_La. They consider the separate contributions of the mass transfer from the two hemispherical caps, and transfer to the liquid flowing down the sides of the bubble. The channel

* Corresponding author. Tel.: +31 20 525 7007; fax: +31 20 525 5604.
E-mail address: R.Krishna@uva.nl (R. Krishna).
[1] Permanent address: The Key Lab of Science and Technology of Controllable Chemical Reactions (MEC), Beijing University of Chemical Technology, Beijing 100029, China.

0009-2509/$ - see front matter © 2005 Elsevier Ltd. All rights reserved.
doi:10.1016/j.ces.2005.01.037

diameter d_c *does* influence the k_La of both cap and film contributions in these fundamental approaches, in contrast to the expectations of Eq. (1). Using extensive CFD simulations of mass transfer in circular capillaries of 1.5, 2 and 3 mm diameters, van Baten and Krishna (2004) also concluded that the dominant contribution to the mass transfer was from the Taylor bubbles to the thin film between the bubble and the wall.

In the present study, we report the results of a comprehensive set of experiments on gas–liquid mass transfer from Taylor bubbles rising in capillaries of diameters in the 1–3 mm range, of both circular and square geometries. The major objective is to verify the applicability of the model of van Baten and Krishna (2004) and to demonstrate the dependence of k_La on the capillary diameter, d_c. Towards this end, the hydrodynamic parameters (Taylor bubble rise velocity, unit cell length, and gas hold-up) were also measured.

2. Experimental set-up

Experiments were carried out in vertical capillaries of square and circular cross-sections listed in Table 1. Seven distinct capillaries were employed, having five different inner dimensions: 1, 2 and 3 mm circular and 1 and 3 mm square. All capillaries were made of Pyrex glass. The experimental set-up shown in Fig. 1 consists of (1) the capillary set-up with an external liquid recirculation loop and (2) an image recording and analysis system. Air was used as the gas phase in all experimental runs with the liquid phase being demineralised water (density = 998 kg/m^3; viscosity = 1 mPa s; surface tension = 72 mN/m). Air and nitrogen were fed from the bottom of the capillary through a T or U bend inlet (refer to Fig. 1 for schematic descriptions). Nitrogen was employed for stripping out dissolved oxygen. All experiments were carried out at room temperature and atmospheric pressure. During experiments, compressed air was fed through a pre-calibrated float-type gas flowmeter. The gas flow provided the driving force for closed-loop liquid recirculation within the system. For a given gas flow rate, the liquid recirculation rate was regulated using a valve placed above a pre-calibrated float-type liquid flowmeter installed within the loop. Gas–liquid disengagement occurred in a zone above the capillary. The volume of liquid in the disengagement zone was kept constant at 10 mL at the start of each experimental run, corresponding to a liquid height of 1 cm as shown in Fig. 1. A *YSI* Model 5331 oxygen electrode, employed for mass transfer measurements, was placed in the gas–liquid disengagement zone. The electrode was connected to a PC via an ammeter and an analogue-to-digital converter card.

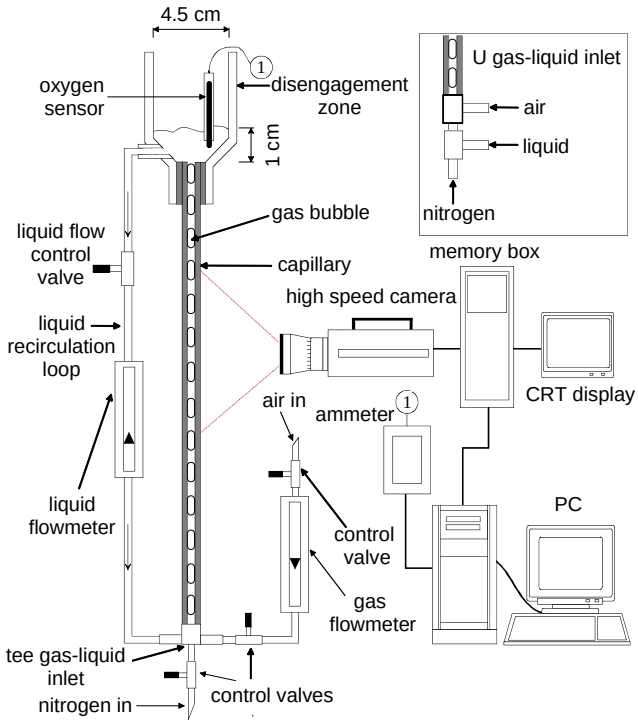

Fig. 1. Schematic representation of the experimental set-up.

Table 1
Description of capillaries used in this study

Geometry	Hydraulic diameter, d_c/[mm]	Length of capillary, L_c/[m]	Inlet nozzle used[a]	Number of experiments
Circular	1	0.2	1 mm U	13
Circular	1	0.47	1 mm U	16
Circular	2	0.45	3 mm U	40
Circular	3	0.45	3 mm U	33
Circular	3	1.4	3 mm T	29
Square	1	0.2	1 mm U	7
Square	3	0.45	3 mm T	38

[a]The dimensions indicated refer to the approximate inner diameters of the gas and liquid nozzles.

The image recording system consists of a *Photron Fastcam-ultima* 40 K high-speed video camera, a memory box and a CRT monitor display. Capable of being set to capture movies at rates of between 30 and 4500 frames per second (fps) in full frame mode and 9000–40 500 fps in segmented frame mode, the high-speed camera was used to obtain quantitative data on bubble rise velocity and bubble frequency. It was positioned mid-way along the capillary height such that it captured rising air bubbles within a convenient vertical distance. Video movies captured by the camera were instantaneously stored in the memory box. The CRT display showed in real-time what was viewed through the camera. Data from the memory box were transferred to the PC for later analysis. Further details on the high-speed video camera set-up are available on our website (Vandu et al., 2004). Video movies on the Taylor flow regime to which this study relates are also available for viewing and downloading.

3. Experimental procedure

3.1. Gas hold-up and unit cell length

The gas hold-up ε_G and unit cell length L_{UC} were determined from analysis of the high-speed movies made during experiments. Once steady state was achieved during a given experimental run, video movies were made for a certain time span which varied with feed gas velocity, at capture rates of between 750 and 4500 fps. From the analysis of each movie made, the bubble frequency f_b defined as the number of bubbles that traverse a given point in the capillary per unit time, was determined. The bubble rise velocity V_b was also determined from the movies by registering the time required for a gas bubble to rise a known distance along the capillary height. Each V_b reported is the average of five values taken, though deviations of more than 4% were hardly observed indicating that flow was steady. With the bubble rise velocity known, the gas hold-up was determined:

$$\varepsilon_G = \frac{U_G}{V_b} \tag{2}$$

where U_G is the superficial gas velocity. For a capillary operated in the upflow mode, Taylor bubbles rise along the capillary height sandwiched between two liquid slugs. Between a gas bubble and the wall of the capillary is a thin downflowing liquid film. We define a unit cell as consisting of a gas bubble and the liquid slug above it. Furthermore, we assume that on average, all unit cells have the same length, with the average unit cell length estimated from

$$L_{UC} = \frac{V_b}{f_b} \tag{3}$$

Based on the assumption that the volume of liquid in the film between a gas bubble and the capillary wall is negligible in comparison to the volume of liquid in the slug, the average liquid slug length L_{slug} can be estimated from the relationship

$$L_{\text{slug}} = L_{UC}(1 - \varepsilon_G) \tag{4}$$

From observations made during the experiments carried out, the assumption of a uniform L_{slug} was found to be justified. This was the case once steady flow was achieved, which often took about a minute or two.

3.2. Mass transfer coefficient

The volumetric mass transfer coefficient k_La was determined by a dynamic oxygen absorption technique (Letzel et al., 1999). The oxygen electrode, placed in the gas–liquid disengagement zone, was used to measure the change in dissolved oxygen concentration. This change in dissolved oxygen concentration was reflected as a change in electrical current displayed on the ammeter to which the electrode was connected, and fed to a PC. The oxygen sensor was made sensitive to the presence of dissolved oxygen by the application of a 0.13 g/mL KCl solution between its tip and an outer membrane made of Teflon. Before the start of each experimental run, the membrane surrounding the tip of the oxygen sensor was changed and the time constant of the sensor k_{sensor} determined by a procedure described in our earlier publication (Vandu and Krishna, 2004). k_{sensor} corresponds to an inherent delay in readings obtained resulting from the fact that the sensor has a finite response time. k_{sensor} values obtained were typically in the range 0.45–0.55 s^{-1}, an order of magnitude higher than the measured k_La per unit volume of dispersion (gas + liquid) in the entire capillary set-up. This meant that the sensor limitation had no noticeable effect on the accuracy of the k_La values reported in this paper. For the determination of k_La in the capillary, dissolved oxygen was stripped from the liquid phase to a negligible concentration by the use of nitrogen. After the stripping operation, air was introduced into the capillary, with the uptake of oxygen into the liquid phase continuously monitored by the sensor. Sufficient time was given in each experimental run for the oxygen saturation concentration in the liquid C_L^* to be reached.

To obtain k_La values from experimental oxygen absorption curves, a model of the capillary set-up was developed based on the following assumptions:

- well-mixed gas and liquid phases in each unit cell,
- plug flow of liquid in the recirculation loop,
- well-mixed liquid phase in the disengagement zone.

The unit cells were assumed to extend to the dispersion height. This meant that gas bubbles and their corresponding volumes of liquid in the gas–liquid disengagement zone were taken as part of the gas–liquid segmented flow in the capillary. The disengagement zone was thus gas free in the model developed, meaning no mass transfer was assumed to occur there. Fig. 2 shows a schematic representation of the model. Eqs. (5)–(9) are the governing model mass balance equations.

Well-mixed gas phase in each unit cell

$$\varepsilon_G \frac{\mathrm{d}(C_{GC})}{\mathrm{d}t} = -U_G \frac{\Delta(C_{GC})}{L_{UC}} - k_La\left(\frac{C_{GC}}{m} - C_{LC}\right) \tag{5}$$

Well-mixed liquid phase in each unit cell

$$\varepsilon_L \frac{\mathrm{d}(C_{LC})}{\mathrm{d}t} = -U_L \frac{\Delta(C_{LC})}{L_{UC}} + k_La\left(\frac{C_{GC}}{m} - C_{LC}\right) \tag{6}$$

Well-mixed liquid phase in the disengagement zone

$$\frac{\mathrm{d}(C_{LD})}{\mathrm{d}t} = -U_{LD} \frac{\Delta(C_{LD})}{H_D} \tag{7}$$

Plug flow of liquid in the recirculation loop

$$\frac{\partial(C_{LR})}{\partial t} = U_{LR} \frac{\partial(C_{LR})}{\partial z} \tag{8}$$

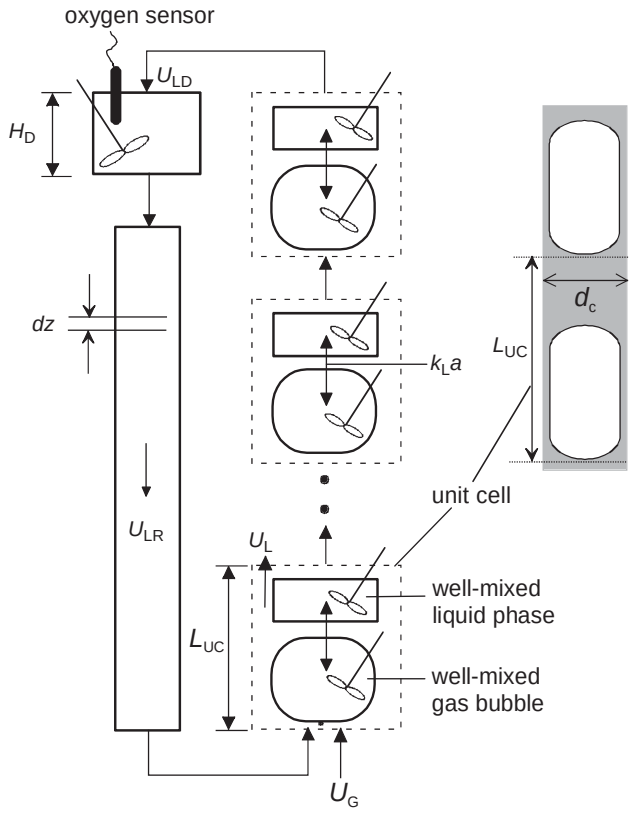

Fig. 2. Schematic representation of the model developed for obtaining k_La values.

Sensor correction equation

$$\frac{\mathrm{d}(C_{\mathrm{sensor}})}{\mathrm{d}t} = k_{\mathrm{sensor}}(C_{LD} - C_{\mathrm{sensor}}) \tag{9}$$

ε_G and ε_L are the gas and liquid hold-ups in the *capillary section* of the set-up, i.e., excluding the gas–liquid disengagement zone and liquid recirculation loop volume. k_La is the volumetric mass transfer coefficient per unit volume of *dispersion* (gas + liquid) in the *capillary section*, where k_L is the liquid side mass transfer coefficient and a is the gas–liquid interfacial area per unit cell volume. U_G is the superficial gas velocity with respect to the capillary cross-section while U_L, U_{LD} and U_{LR} are the superficial liquid velocities in the capillary, disengagement zone and recirculation loop, respectively. H_D is the dispersion height in the disengagement zone and the solubility coefficient of oxygen in water $m = 28$. Eqs. (5)–(9) are subject to the following boundary conditions:

- At time $t = 0$, $C_{GC} = C_{GC,\mathrm{inlet}}$,
- At time $t = 0$, $C_{LC} = C_{LD} = C_{LR} = 0$,
- $C_{LC,\mathrm{in}} = C_{LR,\mathrm{out}}$,
- $C_{LR,\mathrm{in}} = C_{LD,\mathrm{out}}$,
- $C_{LD,\mathrm{in}} = C_{LC,\mathrm{out}}$.

Solving the equations involved discretizing their spatial derivatives using a first-order backward difference approximation. The discretized equations were coded in FORTRAN and solved by the method of lines utilising the ODE solver LSODE (Hindmarsh, 2001) in double precision. Fig. 3 shows a typical experimental oxygen absorption response and the fit obtained using the model developed. The plot is from an experimental run in the 0.2 m long, 1 mm diameter circular capillary with $U_G = 0.099\,\mathrm{m/s}$ and $U_L = 0.085\,\mathrm{m/s}$. k_La obtained is $0.382\,\mathrm{s}^{-1}$. The small bump observed in Fig. 3 at about 350 s in both the experimental and model-predicted curves is due to the first full circulation of the liquid in the capillary set-up.

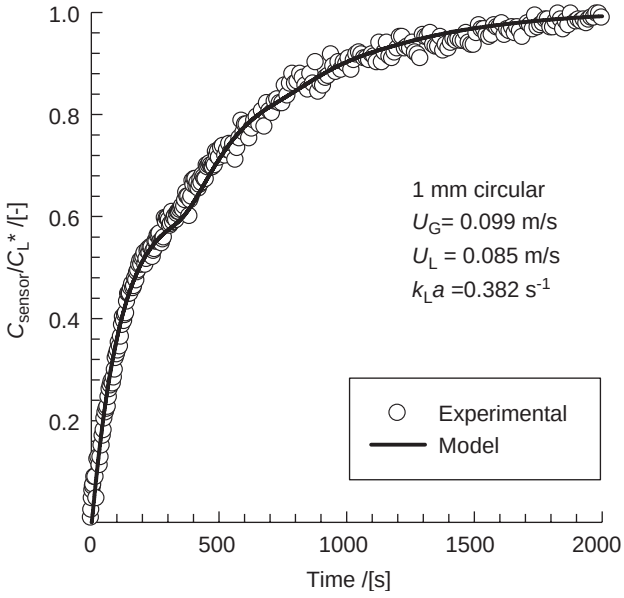

Fig. 3. Typical oxygen absorption dynamics curve and model fit. Data from the 1 mm circular capillary with $L_C = 0.2\,\mathrm{m}$.

4. Results and discussions

Fig. 4a,b and c shows a comparison of experimental k_La data obtained in the 1, 2 and 3 mm capillaries with the k_La predicted using Eq. (1). The diffusivity of methane in water, the system used by Bercic and Pintar (1997), is estimated to be $\mathfrak{D} = 2 \times 10^{-9}\,\mathrm{m}^2/\mathrm{s}$, which is quite close to that of oxygen in water used in our experimental studies, and therefore no further correction for the diffusivity needs to be made. While the Bercic–Pintar correlation underestimates our experimental k_La values in the 1 mm capillaries, it overestimates these for the 2 and 3 mm capillaries. The reasons for the poor predictions due to Eq. (1) are as follows: Firstly, Eq. (1) anticipates no dependence of k_La on channel dimensions. Secondly, the Bercic–Pintar experimental studies were conducted with relatively large unit cell lengths of up to 0.22 m, and for values of $(U_G + U_L)$ generally less than 0.16 m/s, i.e., in studying the effect of the gas bubble and liquid slug lengths on k_La. In contrast, in our experimental studies, L_{UC} ranged from 0.005 to 0.06 m (87% of our data

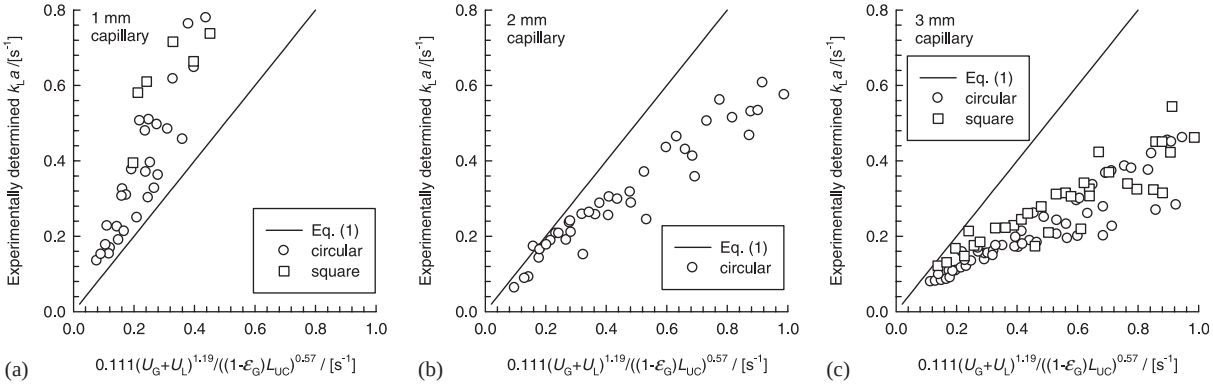

Fig. 4. Comparison of experimental $k_L a$ data with correlation of Bercic and Pintar (1997) given by Eq. (1).

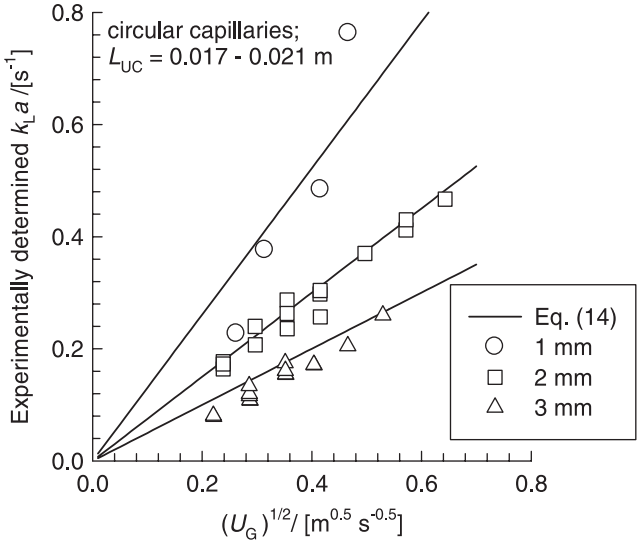

Fig. 5. Experimental $k_L a$ values for 1, 2 and 3 mm circular capillaries plotted against $U_G^{1/2}$. In the chosen data set, the unit cell lengths were in the range $L_{UC} = 0.017$–0.021 m. The straight lines are plotted using Eq. (14) taking $C_1 = 4.5$.

were obtained with $L_{UC} < 0.025$ m) with $(U_G + U_L)$ spanning the much wider range of 0.09–0.65 m/s. For the large unit cell lengths used in their experiments, the film reaches saturation in many of the experiments and is not as effective as short films used in our present study.

In order to underline the dependence of $k_L a$ on the channel dimension d_c, we have selected a set of data on circular capillaries for which the unit cell lengths L_{UC} vary in a relatively narrow range, 0.017–0.021 m. In Fig. 5 the experimental $k_L a$ is plotted against $U_G^{1/2}$ for this restricted data set. The data clearly demonstrate the strong decrease in $k_L a$ with increased channel dimension.

We now consider the more fundamental approach to describe mass transfer from Taylor bubbles developed by van Baten and Krishna (2004). Their model considers two contributions to mass transfer: (1) the caps (assumed to be hemispherical) at either end of the bubble and (2) the liquid film surrounding the bubble. They put forward the following relationship for the overall volumetric mass transfer coefficient:

$$k_L a = k_{L,\mathrm{cap}} a_{\mathrm{cap}} + k_{L,\mathrm{film}} a_{\mathrm{film}} \tag{10}$$

The mass transfer coefficients $k_{L,\mathrm{cap}}$ and $k_{L,\mathrm{film}}$ can be estimated from the Higbie penetration mass transfer model:

$$k_{L,\mathrm{cap}} = 2\sqrt{\frac{2\text{Đ}V_b}{\pi^2 d_c}} \tag{11}$$

$$k_{L,\mathrm{film}} = 2\sqrt{\frac{\text{Đ}}{\pi t_{\mathrm{film}}}} \tag{12}$$

The contact time of the liquid film t_{film}, with the gas bubble can be approximated by the relationship $L_{UC}\varepsilon_G/V_b$. The specific interfacial area of the two hemispherical caps $a_{\mathrm{cap}} = 4/L_{UC}$ while the film specific interfacial area $a_{\mathrm{film}} = 4\varepsilon_G/d_c$. Incorporating the expressions for the specific interfacial areas we obtain

$$k_L a = k_{L,\mathrm{cap}} a_{\mathrm{cap}} + k_{L,\mathrm{film}} a_{\mathrm{film}} = 2\frac{\sqrt{2}}{\pi}\sqrt{\frac{\text{Đ}V_b}{d_c}}\frac{4}{L_{UC}} + \frac{2}{\sqrt{\pi}}\sqrt{\frac{\text{Đ}V_b}{\varepsilon_G L_{UC}}}\frac{4\varepsilon_G}{d_c} \tag{13}$$

van Baten and Krishna (2004) obtained excellent agreement between the predictions of Eq. (13) and CFD simulations of mass transfer from Taylor bubbles in *circular* capillaries of 1.5, 2 and 3 mm with the *idealized* geometry (two hemispherical caps at either end) as assumed in the model development. On the basis of an extensive set of CFD simulations, van Baten and Krishna (2004) concluded that the major contribution to mass transfer was the film contribution $k_{L,\mathrm{film}} a_{\mathrm{film}}$. There is clearly some degree of uncertainty in applying their model to *square* capillaries for which the film thickness along the perimeter cannot be expected to be uniform, being thicker at the edges. Furthermore, the assumption of hemispherical caps at either end of the Taylor bubble may not be entirely true, as is evidenced by the video recordings (Vandu et al., 2004). We therefore adopt a simplified approach in which we take the film contribution, which

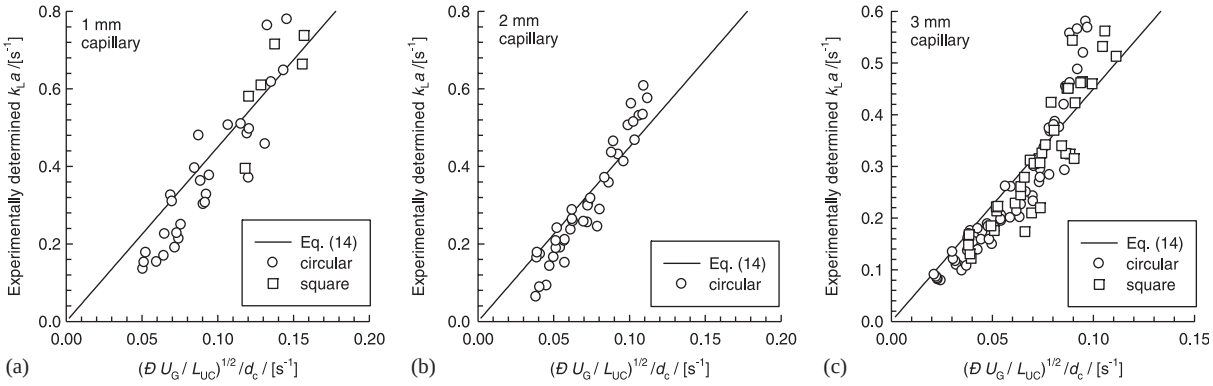

Fig. 6. Experimental volumetric mass transfer coefficient $k_L a$ plotted as function of $\sqrt{(ĐU_G/L_{UC})}1/d_c$ for (a) 1 mm, (b) 2 mm and (c) 3 mm capillaries. The straight lines are drawn using Eq. (14) taking $C_1 = 4.5$.

is assumed to be dominant and simplify Eq. (13) as follows:

$$k_L a = C_1 \sqrt{\frac{ĐU_G}{L_{UC}}}\,\frac{1}{d_c} \tag{14}$$

where we have also used Eq. (2) to eliminate V_b in the film contribution and replacing this with U_G/ε_G and also introducing a constant C_1. The experimental data for the 1, 2 and 3 mm capillaries are plotted against $\sqrt{(ĐU_G/L_{UC})}1/d_c$ in Fig. 6a,b and c. The straight lines in Fig. 6 represent calculations following Eq. (14) taking $C_1 = 4.5$, the best fit value on the basis of a regression of the complete data set; coincidentally this value of C_1 is almost precisely the theoretical value from the model for the film contribution, i.e., $8/\sqrt{\pi}$. The agreement between the model and the experiment is reasonably good for both circular and square capillaries for all three dimensions. The maximum deviation between the model and the experiments is ±30%, with most of the data lying within ±20%. The good agreement between the experimental $k_L a$ data and $k_{L,\mathrm{film}} a_{\mathrm{film}}$ confirms that this contribution is the dominant one for the range of conditions investigated here. Furthermore, the theoretical model is able to capture the dependence of $k_L a$ on d_c; this can be verified from Fig. 5 wherein the straight lines are drawn following Eq. (14).

In an attempt to find a range of applicability of Eq. (14), use is made of the parameter $((U_G + U_L)/L_{\mathrm{slug}})$, which is the ratio of the combined gas and liquid velocity to the liquid slug length. In Fig. 7, a logarithmic plot of $((U_G + U_L)/L_{\mathrm{slug}})^{0.5}$ versus the liquid film contact time t_{film} is depicted for all experimental data points obtained in this study as well as those from the work of Bercic and Pintar (1997). In order to compute t_{film}, the bubble rise velocity is required. Since it was not measured in the Bercic–Pintar experiments, it was estimated using the following correlation developed in an earlier study (Liu et al., 2005):

$$V_b = (U_G + U_L)\left(\frac{1}{1 - 0.61Ca^{0.33}}\right) \tag{15}$$

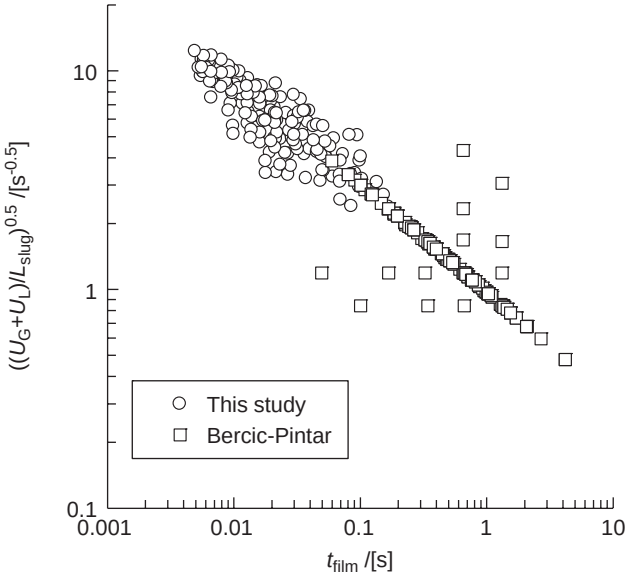

Fig. 7. Comparison of the experimental results obtained in this study with those of Bercic and Pintar (1997) based on a plot of the estimated film contact time versus the parameter $((U_G + U_L)/L_{\mathrm{slug}})^{0.5}$.

where Ca, the capillary number $= (\mu_L(U_G + U_L)/\sigma)$. μ_L is the liquid density and σ the liquid surface tension. From Fig. 7, it is observed that the bulk of the data points from the experimental study presented in this paper relate to $t_{\mathrm{film}} < 0.1$ s. For the Bercic–Pintar experiments, $t_{\mathrm{film}} > 0.1$ s for all but four data points, extending all the way up to 4 s. $((U_G + U_L)/L_{\mathrm{slug}})^{0.5} > 3\,\mathrm{s}^{-0.5}$ corresponds to short film contact times. In this range, the film contribution to mass transfer will be dominant and Eq. (14) can be applied for estimating $k_L a$. On the other hand $((U_G + U_L)/L_{\mathrm{slug}})^{0.5} < 3\,\mathrm{s}^{-0.5}$ relates to the region of large film contact times and a diminished role of the film in gas–liquid mass transfer. This region is where the Bercic–Pintar experiments predominate. The high degree of linearity displayed by the Bercic–Pintar data results

from the fact that L_{slug} and L_{UC} were controlled in their experiments.

5. Conclusions

Gas–liquid mass transfer studies from Taylor bubbles rising in capillaries of circular and square cross-sections were carried out with volumetric mass transfer coefficients k_La computed from experimental oxygen dynamics absorption curves. The following major conclusions can be drawn:

(1) The empirical correlation of Bercic and Pintar (1997) given by Eq. (1) shows large deviations when compared with our experimental data. Firstly, their correlation does not include the influence of the channel dimension. Secondly, their correlation has been set up using experimental data wherein large unit cells were realized and the rise velocity was restricted to values below about 0.16 m/s. This would suggest that for many of the Bercic–Pintar experiments, the film reaches saturation and is not very effective. Our experiments were carried out with shorter films and high rise velocities and in all cases the film is not saturated.
(2) Our experimental k_La values are described reasonably well with the model of van Baten and Krishna (2004), assuming that the dominant contribution is due to the film surrounding the Taylor bubble. Furthermore the model was found to be applicable when $((U_G + U_L)/L_{slug})^{0.5} > 3\,s^{-0.5}$. Below this range a diminished film contribution to mass transfer occurs as the liquid in the film begins approaching saturation.

We recommend the use of Eq. (14) for practical estimation of k_La in the range described. The use of this correlation requires us to estimate the unit cell lengths L_{UC}, gas hold-up ε_G, and rise velocity V_b as a function of the operating conditions and system properties. The estimation of these hydrodynamic parameters is the subject of a companion paper (Liu et al., 2005). There are indications that Eq. (14) can also be applied to estimate k_La for a monolith bundle of capillaries, provided good estimate of the hydrodynamic parameters is available (Vandu et al., 2005a,b).

Notation

a	gas–liquid interfacial area per unit cell volume, m^2/m^3
Ca	capillary number, dimensionless
C_L^*	saturation liquid concentration, mol/m^3 or arbitrary units
C_{GC}	gas phase oxygen concentration in the capillary, mol/m^3
C_{LC}	liquid phase oxygen concentration in the capillary, mol/m^3
C_{LD}	liquid phase oxygen concentration in the disengagement zone, mol/m^3
C_{LR}	liquid phase oxygen concentration in the recirculation loop, mol/m^3
C_{sensor}	liquid phase oxygen concentration indicated by the sensor, arbitrary units
d_c	capillary inner diameter, m
Đ	liquid-phase diffusivity, m^2/s
f_b	bubble frequency, s^{-1}
H_D	dispersion height in the disengagement zone, m
k_L	liquid side mass transfer coefficient, m/s
k_{sensor}	sensor time constant, m/s
L_b	bubble length, m
L_c	length of capillary, m
L_{slug}	liquid slug length, m
L_{UC}	unit cell length, m
m	solubility coefficient of oxygen in water, dimensionless
t	time, s
U_G	superficial gas velocity (with respect to the capillary cross-section), m/s
U_L	superficial liquid velocity in the capillary, m/s
U_{LD}	superficial liquid velocity in the disengagement zone, m/s
U_{LR}	superficial liquid velocity in the recirculation loop, m/s
V_b	bubble rise velocity, m/s

Greek letters

$\Delta(C)$	used in Eqs. (5)–(7) to express a variation in concentration, mol/m^3
ε_G	gas hold-up in the capillary, dimensionless
ε_L	liquid hold-up in the capillary, dimensionless

Subscripts and superscripts

b	refers to Taylor bubble
c	refers to capillary
cap	refers to hemispherical bubble cap
D	refers to gas–liquid disengagement zone
film	refers to liquid film
G	refers to gas phase
in	refers to conditions into a given section of the set-up
inlet	refers to conditions at the inlet of the capillary
L	refers to liquid phase
out	refers to conditions out of a given section of the set-up
R	refers to liquid recirculation loop
UC	refers to unit cell
$*$	refers to saturation concentration

Acknowledgements

We are grateful to Dr. G. Bercic for providing us the experimental data reported in his 1997 paper in electronic format. The Netherlands Foundation for Scientific Research—Chemical Sciences division (NWO-CW) is acknowledged for financial assistance provided.

References

Bercic, G., Pintar, A., 1997. The role of gas bubbles and liquid slug lengths on mass transport in the Taylor flow through capillaries. Chemical Engineering Science 52, 3709–3719.

Hindmarsh, A.C., 2001. Livermore Solver for Ordinary Differential Equations. Lawrence Livermore National Laboratory, Livermore, California: http://www.llnl.gov/CASC/.

Irandoust, S., Andersson, B., 1988. Mass-transfer and liquid-phase reactions in a segmented two-phase flow monolithic catalyst reactor. Chemical Engineering Science 43, 1983–1988.

Irandoust, S., Ertle, S., Andersson, B., 1992. Gas–liquid mass-transfer in Taylor flow through a capillary. Canadian Journal of Chemical Engineering 70, 115–119.

Kreutzer, M.T., 2003. Hydrodynamics of Taylor flow in capillaries and monolith reactors. Ph.D. Thesis, Delft University of Technology. Delft, The Netherlands.

Letzel, H.M., Schouten, J.C., Krishna, R., van den Bleek, C.M., 1999. Gas holdup and mass transfer in bubble column reactors operated at elevated pressure. Chemical Engineering Science 54, 2237–2246.

Liu, H., Vandu, C.O., Krishna, R., 2005. Hydrodynamics of Taylor flow in vertical capillaries: flow regimes, bubble rise velocity, liquid slug length and pressure drop. Industrial & Engineering Chemistry Research, in press.

Stankiewicz, A., 2001. Process intensification in in-line monolithic reactor. Chemical Engineering Science 56, 359–364.

van Baten, J.M., Krishna, R., 2004. CFD simulations of mass transfer from Taylor bubbles rising in circular capillaries. Chemical Engineering Science 59, 2535–2545.

Vandu, C.O., Krishna, R., 2004. Volumetric mass transfer coefficients in slurry bubble columns operating in the churn-turbulent flow regime. Chemical Engineering and Processing 43, 987–995.

Vandu, C.O., Liu, H., Krishna, R., 2004. Taylor Bubble Rise in Circular and Square Capillaries. University of Amsterdam, Amsterdam, The Netherlands: http://ct-cr4.chem.uva.nl/SingleCapillary/, 12 June 2004.

Vandu, C.O., Ellenberger, J., Krishna, R., 2005a. Hydrodynamics and mass transfer in an upflow monolith loop reactor. Chemical Engineering and Processing 44, 363–374.

Vandu, C.O., Ellenberger, J., Krishna, R., 2005b. Hydrodynamics and mass transfer in an upflow monolith loop reactor. Influence of vibration excitement. Chemical Engineering Science 59, 4999–5008.